

Equilibrium Calculation of Gaseous Reactive Systems with Simultaneous Species Adsorption

Mingheng Li *

Abstract

This work focuses on the calculation of chemical equilibrium in a gaseous reactive system with simultaneous single or multiple species adsorption under isothermal and isobaric conditions. Two different algorithms are developed following the minimization of Gibbs free energy and the concept of equilibrium constant, respectively. In either case the problem formulation is converted to a set of nonlinear algebraic equations solved using the Newton-Raphson scheme. An example of steam reforming of ethanol with simultaneous CO₂ adsorption is used to illustrate the proposed approach. It is shown that at $T = 500$ °C and $P = 5$ bar, the removal of carbon in the form of CO₂ should exceed 40% in order to achieve a decent enhancement in hydrogen production and purity. An integrated process that combines the endothermic reforming and the exothermic combustion of CH₄ from the off-gas supplemented with simultaneous CO₂ adsorption in the reforming process yields a theoretical maximum overall conversion rate of 86.3% (the corresponding H₂ purity out of the reformer is 89.4% on wet basis or 96.2% on dry basis) with little or no external heat supply. The analysis in this work is potentially useful in the design and optimization of adsorption enhanced reforming reactors for hydrogen generation and other applicable reactive systems.

Keywords: Equilibrium, Adsorption, Optimization, Hydrogen, Adsorption Enhanced Reforming

1 Introduction

Chemical equilibrium in a reactive system is a state where the chemical activity of each species does not have a net change over time [38]. The calculation of chemical equilibrium provides the thermodynamic limit of a chemical process and has been traditionally used in the design and analysis of chemical equipment such as turbines and engines etc. [17, 44] The advances in chemical equilibrium algorithms have been significantly facilitated by the even-increasing computational power of modern computers. One milestone in chemical equilibrium calculation is the development of the NASA chemical equilibrium and applications (CEA) code, which is capable of tracking hundreds of species in a gaseous reactive system and has been used in various applications such as rockets, incident/reflected shocks and Chapman-Jouguet detonations etc. [13]. The so-called Gibbs reactor module that is based on the minimization of Gibbs free energy has also been incorporated in various

*Department of Chemical and Materials Engineering, California State Polytechnic University, Pomona, CA 91768 USA. Tel: +1-909-869-3668. Fax: +1-909-869-6920. E-mail: minghengli@csupomona.edu.

modern engineering solvers including Pro/II[®] and Aspen Hysys[®] to predict equilibrium compositions [3,18]. Nowadays thermodynamic analyses based on chemical equilibrium calculations have been found in a variety of applications such as material interfacial phenomena [35,37,46], biological processes [11,22,40], and reacting nozzle flows [27] to name a few.

More recently, researchers in various groups have shown a great interest in the application of chemical equilibrium to processes related to hydrogen generation and fuel cells [4,5,7,10,28–31,33]. As reducing the demand on fossil resources has been a public concern, hydrogen, being a potential carrier of clean energy, is now an important research topic that may lead into a new energy era. The production of hydrogen can be realized through various routes such as steam reforming of hydrocarbon [15], gasification of coal [39], chemical looping combustion of coal [14], and water splitting through thermochemical cycle [41] etc. In particular, hydrogen generation from biomass has caught lots of attention as it is a potentially viable, renewable and carbon-neutral (or even carbon-negative in conjunction with sequestration) process [8]. Most of these processes involve water gas shift reaction ($\text{CO} + \text{H}_2\text{O} = \text{CO}_2 + \text{H}_2$). If CO_2 can be simultaneously removed as the water gas shift reaction proceeds, the thermodynamic limitation can be circumvented and therefore, the chemical equilibrium shifts to the right, resulting in an enhancement in the extent of the forward reaction and the hydrogen yield.

This work focuses on the development of algorithms for chemical equilibrium calculations in gaseous reactive systems with simultaneous single or multiple species adsorption. The algorithms are then applied to the thermodynamic analysis of steam reforming of ethanol. Implications to an integrated autothermal process for hydrogen generation from steam reforming of hydrocarbons are discussed at the end of this work.

2 Chemical equilibrium calculation through nonlinear optimization

For a closed system under constant temperature and pressure, the Gibbs free energy decreases as equilibrium is approached. Therefore, one approach to equilibrium calculation in an isothermal and isobaric reactive system is to minimize its total Gibbs free energy. The mathematical formulation generally leads to a nonlinear optimization problem which can be solved using numerical methods. This approach is advantageous over the equilibrium constant method when simultaneously tracking a large number of species is necessary because it circumvents specifying a set of reactions a priori. To this end, it is worth noting that even though the NASA CAE package is capable of handling various types of equilibrium calculations, no species adsorption is explicitly accounted for in the current code [13].

The focus of this work is to calculate the chemical equilibrium of a reactive gaseous system with species adsorption, which is a common problem to adsorption enhanced reactive systems [9,16,23,24,47,48]. In the problem formulation, the following assumptions are made: (1) the reactive system is maintained at isothermal and isobaric conditions; (2) the gaseous phase obeys

the ideal gas law; (3) there is no heterogeneous reaction on the surface of the adsorbent; and (4) there is no condensed species in the entire reactive system. Consider such a reactive system with one kilogram of reactants, the Gibbs free energy (G) of the entire reactive system is

$$G = \sum_{j=1}^s (\mu_j^{(g)} n_j^{(g)} + \mu_j^{(ads)} n_j^{(ads)}) \quad (1)$$

where s is the total number of species, n_j is the amount of species j in mole, μ is the chemical potential, and the superscripts (g) and (ads) stand for properties related to species in the gas phase and on the surface, respectively. When equilibrium is reached, the following criteria should be satisfied:

$$\mu_j^{(ads)} = \mu_j^{(g)} \quad (j = 1, \dots, s) \quad (2)$$

For a gaseous species that obeys ideal gas law, its chemical potential can be calculated using the following equation [38]:

$$\mu_j^{(g)} = \mu_j^{0(g)} + RT \ln \frac{P}{P^0} + RT \ln n_j^{(g)} / n_T^{(g)} \quad (j = 1, \dots, s) \quad (3)$$

where T and P are temperature and pressure of the system, respectively, R is the gas constant (8.314 J/mol/K), 0 stands for properties under standard conditions ($P^0 = 1$ bar), and $n_T^{(g)} = \sum_{j=1}^s n_j^{(g)}$. However, a detailed expression for $\mu_j^{(ads)}$ might not be necessary because the relationship between the gaseous species and the adsorbed species can sometimes be experimentally obtained. Based on the Langmuir isotherm widely used in the analysis of adsorption phenomena [21] or experimental observations (e.g., equilibrium chemisorption isotherms of CO₂ on hydrotalcites [10, 24]), the adsorption/desorption equilibrium typically follows the relationship below:

$$n_j^{(ads)} = \frac{S n_{j,sat}^{(ads)} \beta_j P_j}{1 + \sum_{j=1}^s \beta_j P_j} = \frac{S n_{j,sat}^{(ads)} \beta_j \frac{n_j^{(g)}}{n_T^{(g)}} P}{1 + \sum_{j=1}^s \beta_j \frac{n_j^{(g)}}{n_T^{(g)}} P} \quad (j = 1, \dots, s) \quad (4)$$

where $n_j^{(ads)}$ is the actual adsorbed amount of species j in mole, $n_{j,sat}^{(ads)}$ is the saturated surface concentration in mole/m², S is the total surface area of the adsorbent, β_j is a constant for species j under isothermal conditions, P_j is the partial pressure of species j in the gas phase. Based on Eq.4, the ratio of $n_j^{(ads)}$ to $n_j^{(g)}$ is expressed as follows:

$$r_j = \frac{n_j^{(ads)}}{n_j^{(g)}} = \frac{S n_{j,sat}^{(ads)} \beta_j P}{n_T^{(g)} + \sum_{j=1}^s \beta_j n_j^{(g)} P} \quad (j = 1, \dots, s) \quad (5)$$

There are two ways to solve the relationship between the equilibrium composition and the amount of adsorbent. One could start with the surface area of the adsorbent and include Eq.4

in the optimization problem to solve the equilibrium composition. Alternatively, one could start with r_j and solve the equilibrium composition from the optimization problem. The surface area of the adsorbent is then calculated based on Eq.5 and the equilibrium composition. The latter approach is used in this work because the number of constraints can be significantly reduced in the optimization problem. However, it is important to note that r_j are not independent if multiple species are adsorbed simultaneously. In such a case, r_j should be specified based on the following relationship:

$$\frac{r_i}{r_j} = \frac{n_{i,sat}^{(ads)} \beta_i}{n_{j,sat}^{(ads)} \beta_j} \quad (6)$$

To minimize the Gibbs free energy of the entire system described by Eq.1, the mass balance should be satisfied at the same time. This is achieved by the so-called atomic balance equations [26]. Let a_{ij} be the number of chemical element i contained in species j , the atomic balance equation is

$$\sum_{j=1}^s a_{ij} n_j^{(g)} + \sum_{j=1}^s a_{ij} n_j^{(ads)} = \sum_{j=1}^s a_{ij} n_j^{(g)}(0) \quad (i = 1, \dots, \epsilon) \quad (7)$$

where ϵ is the total number of chemical elements in this reactive system. $b_i(0) = \sum_{j=1}^s a_{ij} n_j^{(g)}(0)$ is the number of moles of elements i per kilogram reactants. It is worth noting that the effective number of equations in Eq.7 is equal to the rank of the atomic matrix, which might be less than ϵ occasionally. In such a case, Eq.7 should be replaced by its minimum realization. Interested readers are directed to open literature for more details [26]. However, the optimization algorithms can still be developed in a similar manner.

Based on the above analysis, the calculation of equilibrium compositions is formulated as the following nonlinear optimization problem:

$$\begin{aligned} \min_{n_j^{(g)}, n_j^{(ads)}} G &= \sum_{j=1}^s (\mu_j^{(g)} n_j^{(g)} + \mu_j^{(ads)} n_j^{(ads)}) \\ &s.t. \\ 0 &= \sum_{j=1}^s a_{ij} n_j^{(g)} + \sum_{j=1}^s a_{ij} n_j^{(ads)} - b_i(0) \quad (i = 1, \dots, \epsilon) \\ \mu_j^{(ads)} &= \mu_j^{(g)} \quad (j = 1, \dots, s) \\ \frac{n_j^{(ads)}}{n_j^{(g)}} &= r_j \quad (j = 1, \dots, s) \\ \mu_j^{(g)} &= \mu_j^{0(g)} + RT \ln \frac{P}{P_0} + RT \ln n_j^{(g)} / n_T^{(g)} \quad (j = 1, \dots, s) \\ n_T^{(g)} &= \sum_{j=1}^s n_j^{(g)} \end{aligned} \quad (8)$$

Eq.8 can be simplified by canceling the terms related to the adsorbed species. The resulting problem is:

$$\begin{aligned}
\min_{n_j^{(g)}} G &= \sum_{j=1}^s (1 + r_j) \mu_j^{(g)} n_j^{(g)} \\
s.t. & \\
0 &= \sum_{j=1}^s (1 + r_j) a_{ij} n_j^{(g)} - b_i(0) \quad (i = 1, \dots, \epsilon) \\
\mu_j^{(g)} &= \mu_j^{0(g)} + RT \ln \frac{P}{P_0} + RT \ln n_j^{(g)} / \sum_{j=1}^s n_j^{(g)} \quad (j = 1, \dots, s) \\
n_T^{(g)} &= \sum_{j=1}^s n_j^{(g)}
\end{aligned} \tag{9}$$

Strictly speaking, inequity constraints $n_j \geq 0$ ($j = 1, \dots, s$) should be included in the optimization problem described by Eq.8 or 9. This is handled by solving $\ln n_j$ instead of n_j [13] in the detailed solution procedure. Even when this strategy is applied, sometimes n_j can still be very close (or theoretically equal) to zero during the iterations and singularity problems occur when taking logarithms of extremely small positive numbers. These can be avoided by purposely setting the minimum of n_j to a very small number (e.g., 10^{-100}) in this work. Any n_j that is smaller than its minimum will be replaced by its lower limit during the iterations. Such a modification does not have an effect on the accuracy of the solution because the contribution of $n_j \mu_j$ of these components to the total Gibbs free energy would be very close to zero (Note that $\lim_{n_j \rightarrow 0} n_j \ln n_j = -\lim_{n_j \rightarrow 0} n_j = 0$ based on L'Hopital's rule). With this in mind, the optimization problem described in Eq.9 is then converted to a set of nonlinear algebraic equations using the Lagrangian multiplier method. First we define $f = \sum_{j=1}^s (1 + r_j) \mu_j^{(g)} n_j^{(g)} + \sum_{i=1}^{\epsilon} \lambda_i \left[\sum_{j=1}^s (1 + r_j) a_{ij} n_j^{(g)} - b_i(0) \right]$, where λ_i are the Lagrangian multipliers, the optimal solution to the optimization problem of Eq.9 should be determined by solving the following nonlinear algebraic equations:

$$\begin{aligned}
0 &= \frac{\partial f}{\partial n_j} = (1 + r_j) \mu_j^{(g)} + \sum_{i=1}^{\epsilon} (1 + r_j) a_{ij} \lambda_i \quad (j = 1, \dots, s) \\
0 &= \frac{\partial f}{\partial \lambda_i} = \sum_{j=1}^s (1 + r_j) a_{ij} n_j^{(g)} - b_i(0) \quad (i = 1, \dots, \epsilon) \\
\mu_j^{(g)} &= \mu_j^{0(g)} + RT \ln \frac{P}{P_0} + RT \ln n_j^{(g)} / n_T^{(g)} \quad (j = 1, \dots, s) \\
n_T^{(g)} &= \sum_{j=1}^s n_j^{(g)}
\end{aligned} \tag{10}$$

The variables to be determined are $n_j^{(g)}$ ($j = 1, \dots, s$), λ_i ($i = 1, \dots, \epsilon$) and $n_T^{(g)}$. The $s + \epsilon + 1$ nonlinear algebraic equations in Eq.10 can be solved using the decent Newton-Raphson method.

The central idea of the Newton-Raphson method is to apply multi-variable Taylor series expansion to a nonlinear vector function and then use truncated terms that contain only the first order derivatives to build a linear iterative formula. The formula can be then used to compute the solution with an given initial guess close to the solution; interested readers may refer to specialized books for details (e.g., [34]). Following a method provided in [13], the iterative variables are chosen to be $\Delta \ln n_j^{(g)}$ ($j = 1, \dots, s$), $\Delta \ln n_T^{(g)}$ and $\pi_i = -\lambda_i/RT$ ($i = 1, \dots, \epsilon$) in order to avoid taking the logarithm of negative numbers in the iteration procedure. Note here $\pi_i = -\lambda_i/RT$ is solved directly at each iteration step.

With the definition of π_i , the first equation in Eq.10 can be converted to a dimensionless form as follows:

$$(1 + r_j) \frac{\mu_j^{(g)}}{RT} - \sum_{i=1}^{\epsilon} (1 + r_j) a_{ij} \pi_i = 0 \quad (j = 1, \dots, s) \quad (11)$$

which has the following Newton-Raphson iterative formula:

$$\frac{(1 + r_j) \mu_j^{(g)}}{RT} - \sum_{i=1}^{\epsilon} (1 + r_j) a_{ij} \pi_i - \frac{\partial \left[\frac{(1 + r_j) \mu_j^{(g)}}{RT} \right]}{\partial \ln n_T} \Delta \ln n_T^{(g)} + \frac{\partial \left[\frac{(1 + r_j) \mu_j^{(g)}}{RT} \right]}{\partial \ln n_j} \Delta \ln n_j^{(g)} = 0 \quad (j = 1, \dots, s) \quad (12)$$

or

$$\Delta \ln n_j^{(g)} = -\frac{\mu_j^{(g)}}{RT} + \sum_{i=1}^{\epsilon} a_{ij} \pi_i + \Delta \ln n_T^{(g)} \quad (j = 1, \dots, s) \quad (13)$$

Similarly, the Newton-Raphson iterative formulas for the other equations can be determined as follows:

$$\sum_{j=1}^s (1 + r_j) a_{ij} n_j^{(g)} - \sum_{j=1}^s a_{ij} n_j^{(g)}(0) + \sum_{j=1}^s (1 + r_j) a_{ij} n_j^{(g)} \Delta \ln n_j^{(g)} = 0 \quad (i = 1, \dots, \epsilon) \quad (14)$$

and

$$\sum_{j=1}^s n_j^{(g)} - n_T^{(g)} + \sum_{j=1}^s n_j^{(g)} \Delta \ln n_j^{(g)} - n_T^{(g)} \Delta \ln n_T^{(g)} = 0 \quad (15)$$

In order to expedite the calculation, especially when a large number of species are present in the reactive system, the so-called ‘‘reduced Gibbs iteration’’ scheme has been proposed to significantly reduce the number of variables in the iteration steps [13]. The idea is to cancel $\Delta \ln n_j^{(g)}$ in Eqs.14 and 15 using the relationship expressed by Eq.13. Consequently, Eqs.14 and 15 are converted to

$$\begin{aligned} & \sum_{k=1}^{\epsilon} \left[\sum_{j=1}^s (1 + r_j) a_{kj} a_{ij} n_j^{(g)} \right] \pi_k + \left[\sum_{j=1}^s (1 + r_j) a_{ij} n_j^{(g)} \right] \Delta \ln n_T^{(g)} \\ & = \left[\sum_{j=1}^s a_{ij} n_j^{(g)}(0) - \sum_{j=1}^s (1 + r_j) a_{ij} n_j^{(g)} + \sum_{j=1}^s (1 + r_j) a_{ij} n_j^{(g)} \frac{\mu_j^{(g)}}{RT} \right] \quad (i = 1, \dots, \epsilon) \end{aligned} \quad (16)$$

and

$$\sum_{k=1}^{\epsilon} \left[\sum_{j=1}^s a_{kj} n_j^{(g)} \right] \pi_k + \left[\sum_{j=1}^s n_j^{(g)} - n_T^{(g)} \right] \Delta \ln n_T^{(g)} = \left[n_T^{(g)} - \sum_{j=1}^s n_j^{(g)} + \sum_{j=1}^s n_j^{(g)} \frac{\mu_j^{(g)}}{RT} \right] \quad (17)$$

After the above transformations, the number of variables reduces from $s + \epsilon + 1$ to $\epsilon + 1$, which is favorable when a large amount of species are to be tracked simultaneously. It can be readily verified that the algorithm reduces to the standard NASA CEA one when there is no adsorption, or $r_j = 0$ (for $j = 1, \dots, s$) [13].

The procedure of the calculation is to calculate the terms on the right hand side of Eqs.16 and 17 with initial guesses of $n_j^{(g)}$ and $n_T^{(g)}$, and then solve $\Delta \ln n_T^{(g)}$ and π_k ($k = 1, \dots, \epsilon$) using these $\epsilon + 1$ linear equations. Subsequently, $\Delta \ln n_j^{(g)}$ ($j = 1, \dots, s$) are calculated using Eq.13 based on the value of $\Delta \ln n_T^{(g)}$. The following formulas

$$\begin{aligned} (n_j^{(g)})^{(m+1)} &= \exp \left[(\ln n_j^{(g)})^{(m)} + \alpha^{(m)} \Delta (\ln n_j^{(g)})^{(m)} \right] \quad (j = 1, \dots, s) \\ (n_T^{(g)})^{(m+1)} &= \exp \left[(\ln n_T^{(g)})^{(m)} + \alpha^{(m)} \Delta (\ln n_T^{(g)})^{(m)} \right] \end{aligned} \quad (18)$$

are then applied to update $n_j^{(g)}$ and $n_T^{(g)}$ to be used in the next iteration step. When the composition is far from equilibrium, a positive α that is smaller than one should be chosen to avoid divergence. When it is close to equilibrium, α is set to be 1. The readers may refer to [13] for more detailed discussions.

In the above equations, the thermodynamic data of each species at temperature T , such as the heat capacity, enthalpy, entropy and chemical potential are calculated as functions of temperature [13]:

$$\begin{aligned} \frac{c_p^0(T)}{R} &= \frac{a_1}{T^2} + \frac{a_2}{T} + a_3 + a_4 T + a_5 T^2 + a_6 T^3 + a_7 T^4 \\ \frac{H^0(T)}{RT} &= -\frac{a_1}{T^2} + \frac{a_2}{T} \ln T + a_3 + \frac{a_4}{2} T + \frac{a_5}{3} T^2 + \frac{a_6}{4} T^3 + \frac{a_7}{5} T^4 + \frac{a_8}{T} \\ \frac{S^0(T)}{R} &= -\frac{a_1}{2T^2} - \frac{a_2}{T} + a_3 \ln T + a_4 T + \frac{a_5}{2} T^2 + \frac{a_6}{3} T^3 + \frac{a_7}{4} T^4 + a_9 \\ \frac{\mu_j^{0(g)}}{RT} &= \frac{H^0(T)}{RT} - \frac{S^0(T)}{R} \end{aligned} \quad (19)$$

where a_1, \dots, a_9 are constant for a given species.

3 Chemical equilibrium calculation using the equilibrium constant method

Different from the Gibbs minimization method presented in the previous section, the Gibbs energy of the adsorbed species is not required if the amount ratios r_j are available. However, a set of gaseous reactions should be specified before the concept of equilibrium constant can be applied. A

minimum number of reactions can be determined using a set of independent gaseous reactions such that any gaseous reaction in this reactive system can be expressed by a linear sum of these basis reactions [1]. The minimum number of independent chemical reactions in a reactive system is equal to the number of species minus the rank of the atomic matrix, provided that the former is greater than the latter [26]. For example, if the rank of the atomic matrix is e , the number of independent reactions is $s - e$. In most cases $e = \epsilon$. Occasionally $e < \epsilon$ when not all the row vectors in the atomic matrix are independent.

Consider a small change in the Gibbs free energy in the gaseous phase under isothermal and isobaric conditions:

$$\delta G^{(g)} = \sum_{j=1}^s \mu_j^{(g)} \delta n_j^{(g)} = \sum_{j=1}^s \mu_j^{(g)} \sum_{i=1}^{s-e} \nu_{ij} \delta \xi_i \quad (20)$$

where ν_{ij} is the stoichiometric coefficient of species j and ξ_i is the reaction extent in the i -th reaction, $\delta G^{(g)} = 0$ for any $\delta \xi_i$ at chemical equilibrium implies

$$\sum_{j=1}^s \mu_j^{(g)} \nu_{ij} = 0 \quad (i = 1, \dots, s - e) \quad (21)$$

A combination of Eqs.3 and 21 yields

$$\sum_{j=1}^s \nu_{ij} \left[\frac{\mu_j^{0(g)}}{RT} + \ln \frac{P}{P^0} + \ln \frac{n_j^{(g)}}{n_T^{(g)}} \right] = 0 \quad (i = 1, \dots, s - e) \quad (22)$$

or

$$\prod_{j=1}^s \left[\frac{P n_j^{(g)}}{P^0 n_T^{(g)}} \right]^{\nu_{ij}} = \exp \left[\sum_{j=1}^s \left(-\nu_{ij} \frac{\mu_j^{0(g)}}{RT} \right) \right] = K_{p_i} \quad (i = 1, \dots, s - e) \quad (23)$$

which is just the so-called equilibrium constant method [38].

The Newton-Raphson iterative formula for Eq.22 is

$$\sum_{j=1}^s \nu_{ij} \Delta \ln n_j^{(g)} - \left(\sum_{j=1}^s \nu_{ij} \right) \Delta \ln n_T = - \sum_{j=1}^s \nu_{ij} \frac{\mu_j^{(g)}}{RT} \quad (i = 1, \dots, s - e) \quad (24)$$

As a result, the chemical equilibrium can be solved based on Eqs.14, 15 and 24 (Note that the effective number of equations in Eqs.14 is e if $e < \epsilon$. Therefore, the number of variables is equal to the number of equations). The iterative variables are $\Delta \ln n_j^{(g)}$ ($j = 1, \dots, s$) and $\Delta \ln n_T^{(g)}$. A solution procedure similar to the one presented in section 2 can be followed.

4 A case study - steam reforming of ethanol with simultaneous CO₂ adsorption

A reactive system consisting of steam and ethanol is studied in this section. The steam reforming of biomass-generated ethanol would be a potentially viable and renewable process for hydrogen

production [2, 8, 12]. Experimental studies have shown that for a system of hydrocarbon (e.g., methane, methanol or ethanol) and steam, the yield and purity of hydrogen can be significantly improved if CO_2 is adsorbed [16, 20, 32, 42, 45, 47]. Calculations in this section will provide a quantitative analysis of the underlying physicochemical behavior.

In this reactive system, $T = 500$ °C and $P = 5$ bar and the feed ratio of $\text{C}_2\text{H}_5\text{OH}$ and H_2O is 1 to 3, which are from open literature [36]. The species to be tracked in the systems are CH_4 , CO , CO_2 , C_2H_4 , $\text{C}_2\text{H}_5\text{OH}$, CH_3CHO , H_2 , H_2O and O_2 . The formation of byproducts such as C_2H_4 , CH_3CHO and CH_4 has been observed in the ethanol reforming processes under certain conditions [8, 36]. However, only CH_4 is shown to have a differentiable concentration under the operating conditions in this work. CO_2 is assumed to be the only species that is adsorbed on the surface (i.e., only r_{CO_2} can be a nonzero number) even though the adsorption of multiple species can be readily handled with little extra computational effort. A list of the thermodynamic coefficients, the atomic matrix, and the reaction stoichiometric coefficient matrix (required only in the method based on the equilibrium constant) are shown in Tables 1, 2 and 3 respectively.

The conversion rate of ethanol to hydrogen with simultaneous CO_2 adsorption is solved using the algorithms presented in sections 2 and 3. Computer simulations demonstrate that both algorithms end up with the same results. Typically, it takes only seconds to finish hundreds of simulations. For steam reforming of ethanol, the ideal overall reaction would be $\text{C}_2\text{H}_5\text{OH} + 3 \text{H}_2\text{O} = 6 \text{H}_2 + 2 \text{CO}_2$, which corresponds to a 100% conversion of $\text{C}_2\text{H}_5\text{OH}$ to H_2 . When CO_2 is adsorbed under different $\text{CO}_2^{(\text{ads})}/\text{CO}_2^{(\text{g})}$ ratios, the H_2 yield is shown in Figure 1. Note that the horizontal axis is chosen to be $r_{\text{CO}_2} = \text{CO}_2^{(\text{ads})}/\text{CO}_2^{(\text{g})}$ instead of $\text{CO}_2^{(\text{ads})}$ because the former is roughly proportional to the amount of adsorbent, and therefore, the size of the reactor (See Figure 2 for a plot generated based on Eq.5 and the results from the equilibrium calculation. β_{CO_2} under the operating conditions in this work is estimated to be 22 bar^{-1} based on the experimental data of promoted hydrotalcites [25]). It is seen that with no or little CO_2 adsorption, the conversion rate of $\text{C}_2\text{H}_5\text{OH}$ to H_2 is only 15.4%, which is consistent with the NASA CEA code [13]. When CO_2 is adsorbed, the conversion can be significantly enhanced. For example, at $\text{CO}_2^{(\text{ads})}/\text{CO}_2^{(\text{g})} = 10^2$, the conversion rate of $\text{C}_2\text{H}_5\text{OH}$ to H_2 is 38.9%, or enhanced by a factor greater than 2 (A list of the composition under these two conditions is shown in Table 4). However, a further improvement in the conversion of $\text{C}_2\text{H}_5\text{OH}$ to H_2 requires a significant increase in $\text{CO}_2^{(\text{ads})}/\text{CO}_2^{(\text{g})}$, or the amount of adsorbent. This can be explained by Figure 3, in which it is shown that as CO_2 is adsorbed on the surface, a further removal of CO_2 from the gas phase becomes more and more difficult.

The gas composition in the product mixture under different $\text{CO}_2^{(\text{ads})}/\text{CO}_2^{(\text{g})}$ ratios is shown in Figure 4. Generally speaking, neither O_2 or $\text{C}_2\text{H}_5\text{OH}$ has a differentiable fraction in the product mixture under the operating conditions of interest. As $\text{CO}_2^{(\text{ads})}/\text{CO}_2^{(\text{g})}$ increases, the fraction of $\text{CO}_2^{(\text{g})}$ rapidly decreases to a minimal level (at $\text{CO}_2^{(\text{ads})}/\text{CO}_2^{(\text{g})} = 10^{1\sim 2}$), beyond which a significant reduction in the $\text{CO}_2^{(\text{g})}$ concentration is not obvious. The low partial pressure of CO_2 in the gas phase makes it difficult for an effective adsorption. In fact, at $\text{CO}_2^{(\text{ads})}/\text{CO}_2^{(\text{g})} > 10^1$ the primary carrier of carbon in the gaseous phase is CH_4 instead of CO or CO_2 . When CO_2 is gradually

adsorbed on the surface, the forward reaction in the reversible water gas shift reaction $\text{CO} + \text{H}_2\text{O} = \text{CO}_2 + \text{H}_2$ is favored. As a result, part of the CH_4 is converted to CO_2 through the methane reforming reaction $\text{CH}_4 + \text{H}_2\text{O} = \text{CO} + 3 \text{H}_2$. In this sense, the entire system behaves like a buffer solution. Due to the coupling of multiple equilibrium phenomena, a complete removal of CO_2 is very difficult.

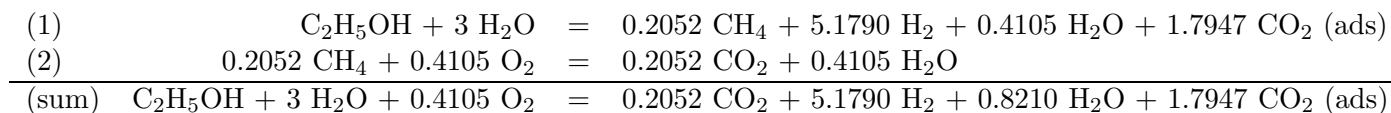
An interesting phenomenon is also observed in this reactive system regarding the specific volume of the product mixture. Note that the calculation is based on a fixed amount of mass of the reactant mixture, and therefore, the volume of the product is proportional to the total amount $n_T^{(g)}$. As shown in Figure 5, the volume of the gas mixture expands about 1.37 times at equilibrium if there is no CO_2 adsorption. According to Le Chatelier’s principle, a low system pressure is preferred for a high conversion of $\text{C}_2\text{H}_5\text{OH}$ to H_2 at chemical equilibrium, which is consistent with experimental observations [36]. When CO_2 is gradually adsorbed on the surface, the volume of the product shrinks. After reaching a minimum at a $\text{CO}_2^{(\text{ads})}/\text{CO}_2^{(\text{g})}$ ratio around 14, the volume of the product increases even as CO_2 is adsorbed. This is because the effect of volume expansion due to methane reforming $\text{CH}_4 + \text{H}_2\text{O} = \text{CO} + 3 \text{H}_2$ is greater than the shrinking effect caused by CO_2 adsorption.

Figure 6 shows the relationship between the conversion rate of $\text{C}_2\text{H}_5\text{OH}$ to H_2 as a function of the CO_2 adsorption ratio, or the absolute amount of CO_2 adsorbed on the surface divided by its theoretical upper limit. It is seen that the enhancement in the H_2 production is not significant when the CO_2 adsorption ratio is below 40% (corresponding to a $\text{CO}_2^{(\text{ads})}/\text{CO}_2^{(\text{g})}$ around 13). This is because the methane reforming reaction and the water gas shift reaction shift only a little to the right, which is reflected by the fact that the total amount drops significantly (Figure 5) and that the fraction of CH_4 and H_2O might even increase (see the peaks in CH_4 and H_2O fractions in Figure 4). As the CO_2 adsorption ratio exceeds 40%, the H_2 production increases linearly (A similar phenomenon is observed in H_2 purity). In such a case, there is little CO_2 or CO in the gas phase (Figure 4), and therefore, the overall reaction in the gas phase is $\text{CH}_4 + 2 \text{H}_2\text{O} = \text{CO}_2 + 4 \text{H}_2$. Because the CO_2 generation rate is roughly balanced by its adsorption rate, 4 mole of H_2 will be generated when 1 mole of CO_2 is removed from the gas phase by adsorption. If the result is interpreted in terms of the H_2 production and CO_2 adsorption ratio, the slope is 4/3 because the ideal reaction is $\text{C}_2\text{H}_5\text{OH} + 3 \text{H}_2\text{O} = 6 \text{H}_2 + 2 \text{CO}_2$.

The reactive system in the above analysis is based on a setting similar to a single stage batch reactor, in which the gas phase has a uniform composition and is in equilibrium with the adsorbent. When multiple stages are used, the reactor performance in terms of hydrogen yield is better. This is because CO_2 , once being adsorbed on the surface, does not have an effect on the reactive system downstream. In the remainder the effect of CO_2 removal is studied using multiple batch reactors in series. This is realized by setting the gas composition at the outlet of one stage to be the inlet composition at the next stage. In addition, the gaseous reactive system at each stage is in local equilibrium with the adsorbent. The H_2 yield and purity are compared with those using a single stage reactor in Figure 7. It is seen that the conversion rate under a fixed total amount of adsorbent is higher when more stages are used (note that the total amount of adsorbent is roughly proportional

to the product of number of stages and $\text{CO}_2^{(\text{ads})}/\text{CO}_2^{(\text{g})}$; see Figure 2 for details). However, the difference among the three cases using multiple stages becomes smaller and smaller as the product of number of stages and $\text{CO}_2^{(\text{ads})}/\text{CO}_2^{(\text{g})}$ becomes sufficiently large. This is encouraging because one might use a finite number of stages to approximate a PFR-type reforming reactor with reasonable accuracy.

In the following studies the $\text{CO}_2^{(\text{ads})}/\text{CO}_2^{(\text{g})}$ is set to be 10^2 at each stage. The evolution of gas composition at each stage is shown in Figure 8. Apparently, the CO_2 and CO fractions are very low and the primary carbon carrier in the gas phase is CH_4 . The hydrogen production increases sharply in the beginning and then slows down as CO_2 is gradually produced from the methane reforming reaction, which is similar to the phenomena shown in Figure 4. Due to the fact that the overall gas phase reaction is strongly endothermic and that a high H_2 production and purity requires a significant amount of adsorbent, an integrated process design could encompass the heat exchange between the endothermic reforming and exothermic combustion of remaining CO and CH_4 in the off-gas downstream of a H_2 separation unit. See Figure 9 for a schematic of this process. $\text{C}_2\text{H}_5\text{OH}$ and H_2O are preheated by the flue gas before entering the reformer, where H_2 is generated and a major part of CO_2 is adsorbed. The product mixture passes through a H_2 separation unit (e.g., a pressure swing adsorption unit, or PSA), where H_2 is separated from unconverted CH_4 , H_2O as well as some CO and CO_2 in trace amount. The CH_4 from the H_2 separation unit is sent to a combustor where heat is supplied to the reformer as well as the feed streams ($\text{C}_2\text{H}_5\text{OH}$ and H_2O) through heat exchange (HE) units. Interested readers might find more discussions in autothermal processes in open literature [6, 8, 15, 19, 43]. A plot of the heat demand by the ethanol reforming and the heat supply through the combustion of the exhaust gases is given in Figure 10. The exit temperature of the combustor is set to be $500\text{ }^\circ\text{C}$. Note that the heat released from the CO_2 adsorption is not taken into account as energy is required for subsequent CO_2 desorption. The calculation does not include the pre-heating of feed streams to $500\text{ }^\circ\text{C}$ or cooling of flue gases to room temperature or the energy required for the H_2 separation unit. Moreover, a 100% efficiency of heat transfer between these two processes is assumed. This rough calculation indicates that a 86.3% theoretical maximum overall conversion of $\text{C}_2\text{H}_5\text{OH}$ to H_2 (the corresponding H_2 purity in the product mixture out of the reformer is 89.4% on wet basis or 96.2% on dry basis, see Table 5 for the composition of other components.) can be achieved with little or no external heat supply in the reforming process if combined with simultaneous CO_2 adsorption. It occurs at the end of the 221st stage if $\text{CO}_2^{(\text{ads})}/\text{CO}_2^{(\text{g})} = 10^2$ at each stage. The reactions in the reforming reactor and the combustor as well as the overall reaction of the entire process ($T = 500\text{ }^\circ\text{C}$) are summarized as follows:



Note that CO and CO_2 in trace amount are not listed above. The net energy demand of the combined reforming and combustion process is zero at $500\text{ }^\circ\text{C}$ if the heat released from CO_2

adsorption is neglected ($\Delta H_1 = -\Delta H_2 = 1.64 \times 10^5$ J/mol. In Figure 10 the heat demand and supply are both 1.64×10^6 J because they are based on 1 kilogram of the ethanol and steam mixture, which contains 10 mole of ethanol and 30 moles of steam). The overall H_2 yield could be less if the heat transfer efficiency and the operating cost are taking into account in this integrated process. A more detailed engineering calculation, which includes regeneration of CO_2 , will be presented in a separate work.

It should be noted that even though the equilibrium calculation can provide a mean-field analysis and predict the upper limit of a reforming process, it is not adequate to mimic the real operation. Due to the continuous nature of a sorption enhanced reforming process, a full understanding requires kinetic models (including the kinetics of reactions and adsorption/desorption as well). Interested readers are directed to open literature (e.g., [9, 47]) for research in this direction.

5 Concluding remarks

Two approaches for the calculation of chemical equilibrium in a gaseous reactive system combined with simultaneous species adsorption are developed in this work following algorithms similar to the NASA CEA code. Both algorithms are very effective in solving a small-scale reactive system with simultaneous species adsorption. Whereas the method based on the concept of equilibrium constants requires specifying a set of independent reactions before the calculation, these reactions are useful in the analysis of various coupled equilibrium phenomena in the entire reactive system.

The algorithms are applied to an enhanced ethanol reforming system where CO_2 is partially or fully removed by adsorption. It is shown that at $T = 500$ °C and $P = 5$ bar, the removal of carbon in the form of CO_2 should exceed 40% in order to achieve a decent enhancement in hydrogen production and purity. Whereas the hydrogen production increases linearly with the CO_2 adsorption ratio if the latter is higher than 40%, the amount of adsorbent (and therefore, the reactor size) required for CO_2 increases exponentially. A trade off between the H_2 production and the reactor size can be achieved by burning CH_4 in the off-gas from the H_2 separation unit to provide heat for the endothermic reforming process. It is shown that a theoretical maximum overall conversion of C_2H_5OH to H_2 around 86.3% can be achieved with little or no external heat supply in the reforming process if combined with simultaneous CO_2 adsorption (the corresponding H_2 purity in the product mixture out of the reformer is 89.4% on wet basis or 96.2% on dry basis).

Even though the adsorption of a single species is discussed in the case study, the algorithms can be potentially applied to multiple species adsorption in a similar manner.

Acknowledgements

This work is partly supported by Intelligent Energy, Inc. (through a DOE subcontract) and the Faculty Center for Professional Development at California State Polytechnic University, Pomona. Industrial feedback from Dr. Durai Swamy and coworkers at Intelligent Energy, Long Beach, CA

and discussions with Drs. T. K. Nguyen and W. Dong are gratefully acknowledged.

References

- [1] R. Aris and R. H. S. Mah. Independence of chemical reactions. *Industrial & Engineering Chemistry Fundamentals*, 2:90–94, 1963.
- [2] L. E. Arteaga, L. M. Peralta, V. Kafarov, Y. Casas, and E. Gonzales. Bioethanol steam reforming for ecological syngas and electricity production using a fuel cell SOFC system. *Chemical Engineering Journal*, 136:256–266, 2008.
- [3] Aspen Technology, Inc. *Hysys 4.0 User Guide*, 2004.
- [4] S. Assabumrungrat, N. Laosiripojana, V. Pavarajarn, W. Sangtongkitcharoen, A. Tangjitmattee, and P. Prasertthdam. Thermodynamic analysis of carbon formation in a solid oxide fuel cell with a direct internal reformer fuelled by methanol. *Journal of Power Sources*, 139:55–60, 2005.
- [5] S. Assabumrungrat, V. Pavarajarn, S. Charojrochkul, and N. Laosiripojana. Thermodynamic analysis for a solid oxide fuel cell with direct internal reforming fueled by ethanol. *Chemical Engineering Science*, 59:6015–6020, 2004.
- [6] M. Baldea and P. Daoutidis. Dynamics and control of autothermal reactors for the production of hydrogen. *Chemical Engineering Science*, 62:3218–3230, 2007.
- [7] C. O. Colpan, I. Dincer, and F. Hamdullahpur. Thermodynamic modeling of direct internal reforming solid oxide fuel cells operating with syngas. *International Journal of Hydrogen Energy*, 32:787–795, 2007.
- [8] G. A. Deluga, J. R. Salge, L. D. Schmidt, and X. E. Verykios. Renewable hydrogen from ethanol by autothermal reforming. *Science*, 303:993–997, 2004.
- [9] Y. Ding and E. Alpay. Adsorption-enhanced steam-methane reforming. *Chemical Engineering Science*, 55:3929–3940, 2000.
- [10] Y. Ding and E. Alpay. Equilibria and kinetics of CO₂ adsorption on hydrotalcite adsorbent. *Chemical Engineering Science*, 55:3461–3474, 2000.
- [11] J. B. Fein, C. J. Daughney, N. Yee, and T. A. Davis. A chemical equilibrium model for metal adsorption onto bacterial surfaces. *Geochimica et Cosmochimica Acta*, 61:3319–3328, 1997.
- [12] N. H. Florin and A. T. Harris. Enhanced hydrogen production from biomass with in situ carbon dioxide capture using calcium oxide sorbents. *Chemical Engineering Science*, 63:287–316, 2008.
- [13] S. Gordon and B. J. McBride. Computer program for calculation of complex chemical equilibrium compositions and applications. Technical Report NASA RP-1311, NASA Lewis Research Center, 1996.

- [14] P. Gupta, L. G. Velazquez-Vargas, F. Li, and L. S. Fan. Chemical looping combustion of coal. In *Proceedings of AIChE Annual Meeting*, New York, 2005. AIChE.
- [15] F. Hershkowitz, P. J. Berlowitz, R. F. Socha, E. Marucchi-Soos, and J. W. Frederick. Hydrogen production via steam reforming in a reverse-flow reactor. In *Proceedings of AIChE Annual Meeting*, New York, 2005. AIChE.
- [16] J. R. Hufton, S. Mayorga, and S. Sircar. Sorption-enhanced reaction process for hydrogen production. *AIChE Journal*, 45:248–256, 1999.
- [17] D. K. Huzel and D. H. Huang. Design of liquid propellant rocket engines. Technical Report NASA SP-125, NASA Lewis Research Center, 1971.
- [18] Invensys Systems, Inc. *Pro/II 8.0 User Guide*, 2006.
- [19] A. A. Iordanidis, P. N. Kechagiopoulos, S. S. Voutetakis, A. A. Lemonidou, and I. A. Vasalos. Autothermal sorption-enhanced steam reforming of bio-oil/biogas mixture and energy generation by fuel cells: Concept analysis and process simulation. *International Journal of Hydrogen Energy*, 31:1058–1065, 2006.
- [20] G. C. Koumpouras, E. Alpay, and F. Stepanek. Mathematical modelling of low-temperature hydrogen production with in situ CO₂ capture. *Chemical Engineering Science*, 62:2833–2841, 2007.
- [21] I. Langmuir. The adsorption of gases on plain surfaces of glass, mica and platinum. *Journal of the American Chemical Society*, 40:1361–1403, 1918.
- [22] M. Lay-Son and C. Drakides. New approach to optimize operational conditions for the biological treatment of a high-strength thiocyanate and ammonium waste: pH as key factor. *Water Research*, 42:774–780, 2008.
- [23] K. B. Lee, M. G. Beaver, H. S. Caram, and S. Sircar. Chemisorption of carbon dioxide on sodium oxide promoted alumina. *AIChE Journal*, 53:2824–2831, 2007.
- [24] K. B. Lee, M. G. Beaver, H. S. Caram, and S. Sircar. Novel thermal-swing sorption-enhanced reaction process concept for hydrogen production by low-temperature steam-methane reforming. *Industrial & Engineering Chemistry Research*, 46:5003–5014, 2007.
- [25] K. B. Lee, A. Verdooren, H. S. Caram, and S. Sircar. Chemisorption of carbon dioxide on potassium-carbonate-promoted hydrotalcite. *Journal of Colloid and Interface Science*, 308:30–39, 2007.
- [26] M. Li. Synthesis of thermodynamically feasible reaction pathways. In *Proceedings of AIChE Annual Meeting*, New York, 2004. AIChE.

- [27] M. Li and P. D. Christofides. Multi-scale modeling and analysis of HVOF thermal spray process. *Chemical Engineering Science*, 60:3649–3669, 2005.
- [28] A. E. Lutz, R. W. Bradshaw, L. Bromberg, and A. Rabinovich. Thermodynamic analysis of hydrogen production by partial oxidation reforming. *International Journal of Hydrogen Energy*, 29:809–816, 2004.
- [29] A. E. Lutz, R. W. Bradshaw, J. O. Keller, and D. E. Witmer. Thermodynamic analysis of hydrogen production by steam reforming. *International Journal of Hydrogen Energy*, 28:159–167, 2003.
- [30] J. A. Matelli and E. Bazzo. A methodology for thermodynamic simulation of high temperature, internal reforming fuel cell systems. *Journal of Power Sources*, 142:160–168, 2005.
- [31] V. Nikulshina, D. Hirsch, M. Mazzotti, and A. Steinfeld. CO₂ capture from air and co-production of H₂ via the Ca(OH)₂-CaCO₃ cycle using concentrated solar power-thermodynamic analysis. *Energy*, 31:1715–1725, 2006.
- [32] A. L. Ortiz and D. P. Harrison. Hydrogen production using sorption-enhanced reaction. *Industrial & Engineering Chemistry Research*, 40:5102–5109, 2001.
- [33] A. Posada and V. Manousiouthakis. Hydrogen and dry ice production through phase equilibrium separation and methane reforming. *Journal of Power Sources*, 156:480–488, 2005.
- [34] W. H. Press, S. A. Teukolsky, W. T. Vetterling, and B. P. Flannery. *Numerical recipes in C++: the art of scientific computing*. Cambridge University Press, New York, USA, 2nd edition, 1997.
- [35] M. M. Rahman. Analysis of simultaneous gas absorption and chemical reaction to a thin liquid film over a spinning disk. *International Communications in Heat and Mass Transfer*, 27:303–314, 2000.
- [36] T. Rampe, P. Hubner, B. Vogel, and A. Heinzl. Hydrogen generation from ethanol by al-
lothermal reforming. In *Proceedings of the First World Conference on Biomass for Energy and Industry*, pages 1889–1892. James & James (Science Publishers) Ltd., 2001.
- [37] Y. K. Rao. Chemical vapour deposition of WSi₂ thin films: Equilibrium W-Si-H-Cl-Ar system. *Journal of Alloys and Compounds*, 452:116–121, 2008.
- [38] S. I. Sandler. *Chemical and Engineering Thermodynamics*. Wiley, New York, 3rd edition, 1999.
- [39] A. Sharma, T. Takanohashi, K. Morishita, T. Takarada, and I. Saito. Low temperature catalytic steam gasification of HyperCoal to produce H₂ and synthesis gas. *Fuel*, 87:491–497, 2008.
- [40] V. V. Smirnov, D. W. Brinkley, M. P. Lanci, K. D. Karlin, and J. P. Roth. Probing metal-mediated O₂ activation in chemical and biological systems. *Journal of Molecular Catalysis A: Chemical*, 251:100–107, 2006.

- [41] A. Steinfeld. Solar thermochemical production of hydrogen - a review. *Solar Energy*, 78:603–615, 2005.
- [42] J. F. Stevens, B. Krishnamurthy, P. Atanassova, and K. Spilker. Development of 50 kW fuel processor for stationary fuel cell applications. DOE Technical Report DOE/GO/13102-1, Chevron Technology Ventures, LLC, 2007.
- [43] T. P. Tiemersma, C. S. Patil, M. van Sint Annaland, and J. A. M. Kuipers. Modelling of packed bed membrane reactors for autothermal production of ultrapure hydrogen. *Chemical Engineering Science*, 61:1602–1616, 2006.
- [44] D. H. Tran and C. A. Snyder. Effects of chemical equilibrium on turbine engine performance for various fuels and combustor temperatures. Technical Report NASA TM-105399, NASA, 1992.
- [45] Y. N. Wang and A. E. Rodrigues. Hydrogen production from steam methane reforming coupled with in situ CO₂ capture: Conceptual parametric study. *Fuel*, 84:1778–1789, 2005.
- [46] Y. S. Won, V. G. Varanasi, O. Kryliouk, T. J. Anderson, L. McElwee-White, and R. J. Perez. Equilibrium analysis of zirconium carbide CVD growth. *Journal of Crystal Growth*, 307:302–308, 2007.
- [47] G. Xiu, P. Li, and A. E. Rodrigues. New generalized strategy for improving sorption-enhanced reaction process. *Chemical Engineering Science*, 58:3425–3437, 2003.
- [48] Z. Yong, V. G. Mata, and A. E. Rodrigues. Adsorption of carbon dioxide on chemically modified high surface area carbon-based adsorbents at high temperature. *Adsorption*, 7:41–50, 2001.

List of Tables

Table 1 Coefficients for thermodynamic properties [13].

Table 2 Atomic matrix.

Table 3 Reaction stoichiometric matrix.

Table 4 Equilibrium composition in the gas phase (the feed is 1 C₂H₅OH + 3 H₂O).

Table 5 Product composition under different conditions.

Table 1: Coefficients for thermodynamic properties [13].

	CH ₄	CO	CO ₂
a_1	-1.766850998E+05	1.489045326E+04	4.943650540E+04
a_2	2.786181020E+03	-2.922285939E+02	-6.264116010E+02
a_3	-1.202577850E+01	5.724527170E+00	5.301725240E+00
a_4	3.917619290E-02	-8.176235030E-03	2.503813816E-03
a_5	-3.619054430E-05	1.456903469E-05	-2.127308728E-07
a_6	2.026853043E-08	-1.087746302E-08	-7.689988780E-10
a_7	-4.976705490E-12	3.027941827E-12	2.849677801E-13
a_8	-2.331314360E+04	-1.303131878E+04	-4.528198460E+04
a_9	8.904322750E+01	-7.859241350E+00	-7.048279440E+00
	C ₂ H ₄	CH ₃ CHO	C ₂ H ₅ OH
a_1	-1.163605836E+05	-1.373904369E+05	-2.342791392E+05
a_2	2.554851510E+03	2.559937679E+03	4.479180550E+03
a_3	-1.609746428E+01	-1.340470172E+01	-2.744817302E+01
a_4	6.625779320E-02	5.922128620E-02	1.088679162E-01
a_5	-7.885081860E-05	-6.240006050E-05	-1.305309334E-04
a_6	5.125224820E-08	3.703324410E-08	8.437346400E-08
a_7	-1.370340031E-11	-9.342697410E-12	-2.234559017E-11
a_8	-6.176191070E+03	-3.318731310E+04	-5.022229000E+04
a_9	1.093338343E+02	1.007417652E+02	1.764829211E+02
	H ₂	H ₂ O	O ₂
a_1	4.078322810E+04	-3.947960830E+04	-3.425563420E+04
a_2	-8.009185450E+02	5.755731020E+02	4.847000970E+02
a_3	8.214701670E+00	9.317826530E-01	1.119010961E+00
a_4	-1.269714360E-02	7.222712860E-03	4.293889240E-03
a_5	1.753604930E-05	-7.342557370E-06	-6.836300520E-07
a_6	-1.202860160E-08	4.955043490E-09	-2.023372700E-09
a_7	3.368093160E-12	-1.336933246E-12	1.039040018E-12
a_8	2.682484380E+03	-3.303974310E+04	-3.391454870E+03
a_9	-3.043788660E+01	1.724205775E+01	1.849699470E+01

Table 2: Atomic matrix.

	CH ₄	CO	CO ₂	C ₂ H ₄	CH ₃ CHO	C ₂ H ₅ OH	H ₂	H ₂ O	O ₂
(C)	1	1	1	2	2	2	0	0	0
(H)	4	0	0	4	4	6	2	2	0
(O)	0	1	2	0	1	1	0	1	2

Table 3: Reaction stoichiometric matrix*.

Reaction No.	CH ₄	CO	CO ₂	C ₂ H ₄	CH ₃ CHO	C ₂ H ₅ OH	H ₂	H ₂ O	O ₂
(1)	-1	-1	0	0	0	1	-1	0	0
(2)	-1	1	0	0	0	0	3	-1	0
(3)	0	-1	1	0	0	0	1	-1	0
(4)	0	2	-2	0	0	0	0	0	1
(5)	0	0	0	0	1	-1	1	0	0
(6)	-2	0	0	1	0	0	2	0	0

* (used only in the equilibrium constant method)

Table 4: Equilibrium composition in the gas phase (Equilibrium composition in the gas phase (the feed is 1 C₂H₅OH + 3 H₂O)).

CO ₂ ^(ads) /CO ₂ ^(g)	CH ₄	CO	CO ₂	C ₂ H ₄	CH ₃ CHO	C ₂ H ₅ OH	H ₂	H ₂ O	O ₂
0	1.2570	0.0489	0.6941	0.0000	0.0000	0.0000	0.9231	2.5629	0.0000
100	0.9773	0.0021	0.0101	0.0000	0.0000	0.0000	2.0888	1.9566	0.0000

Table 5: Product composition under different conditions.

	Post-CO ₂ adsorption (wet)	CO ₂ -H ₂ O free (dry)
H ₂	89.4%	96.2%
CH ₄	3.5%	3.8%
H ₂ O	7.1%	

List of Figures

- Fig.1** Conversion of C_2H_5OH to H_2 (feed mole ratio = $1/3$, $P = 5$ bar and $T = 500$ °C).
- Fig.2** Relationship between $CO_2^{(ads)}/CO_2^{(g)}$ and the surface area of adsorbent (feed mole ratio = $1/3$, $P = 5$ bar and $T = 500$ °C).
- Fig.3** Actual adsorption ratio of CO_2 by the adsorbent (feed mole ratio = $1/3$, $P = 5$ bar and $T = 500$ °C).
- Fig.4** Composition of the gas mixture after reaction (feed mole ratio = $1/3$, $P = 5$ bar and $T = 500$ °C).
- Fig.5** Volume expansion (the volume ratio of the product mixture to the reactant mixture) with respect to the reactant mixture (feed mole ratio = $1/3$, $P = 5$ bar and $T = 500$ °C).
- Fig.6** H_2 yield and purity as functions of the CO_2 adsorption ratio (feed mole ratio = $1/3$, $P = 5$ bar and $T = 500$ °C).
- Fig.7** Conversion of C_2H_5OH to H_2 (feed mole ratio = $1/3$, $P = 5$ bar and $T = 500$ °C) using different number of stages and $CO_2^{(ads)}/CO_2^{(g)}$ ratios.
- Fig.8** Composition of the gas mixture after reaction (feed mole ratio = $1/3$, $P = 5$ bar and $T = 500$ °C) using multiple stages ($CO_2^{(ads)}/CO_2^{(g)}$ is set to be 10^2 at each stage).
- Fig.9** Integrated endothermic reforming and the exothermic combustion of unconverted CH_4 with simultaneous CO_2 in the ethanol reforming process.
- Fig.10** Heat demand by ethanol reforming v.s. heat supply through combustion of exhausting gases from the H_2 separation unit (feed mole ratio = $1/3$, $P = 5$ bar and $T = 500$ °C, $CO_2^{(ads)}/CO_2^{(g)} = 10^2$ at each stage).

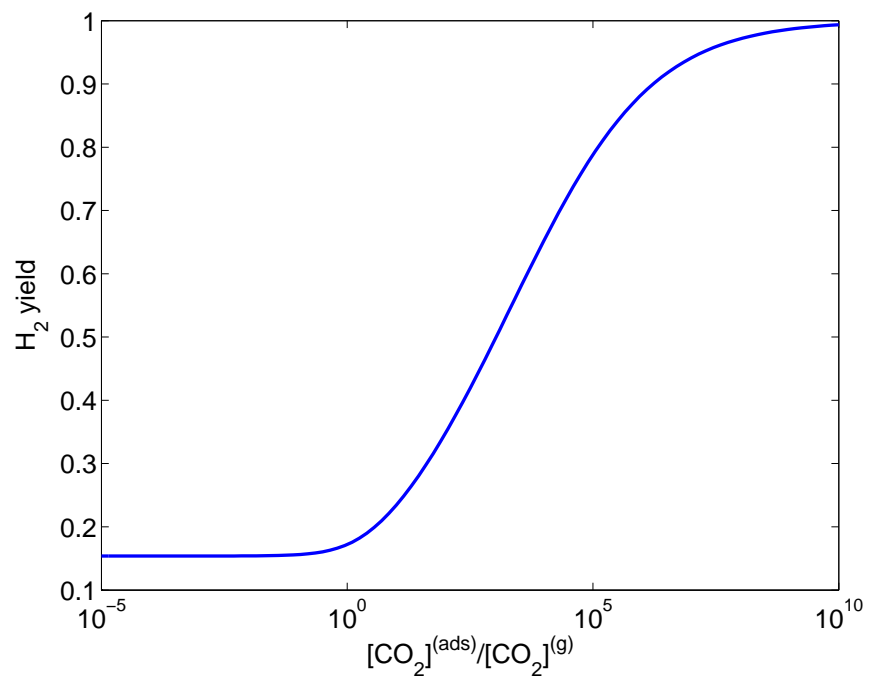


Figure 1: Conversion of C₂H₅OH to H₂ (feed mole ratio = 1/3, P = 5 bar and T = 500 °C).

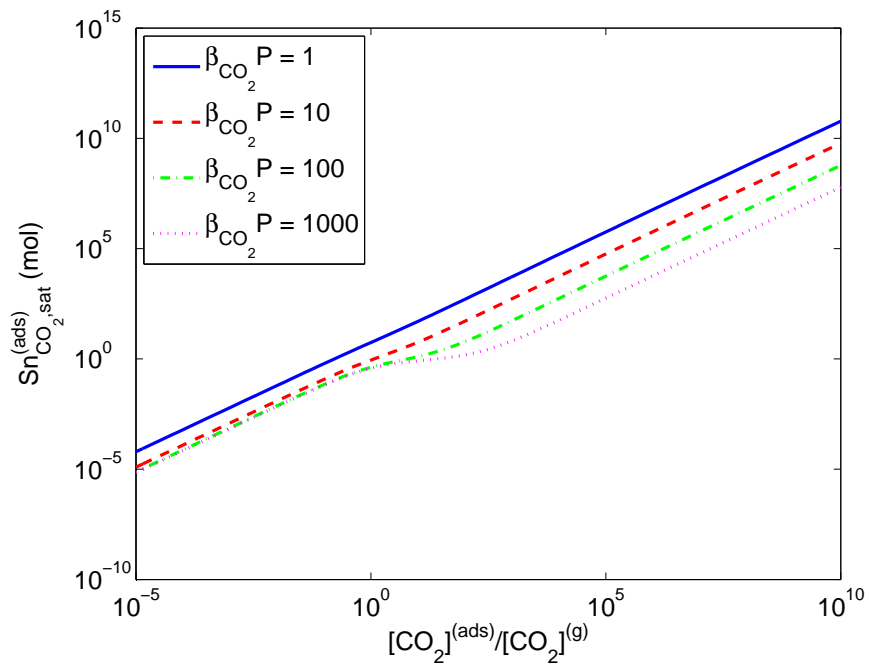


Figure 2: Relationship between $CO_2^{(ads)}/CO_2^{(g)}$ and the surface area of adsorbent (feed mole ratio = 1/3, P = 5 bar and T = 500 °C).

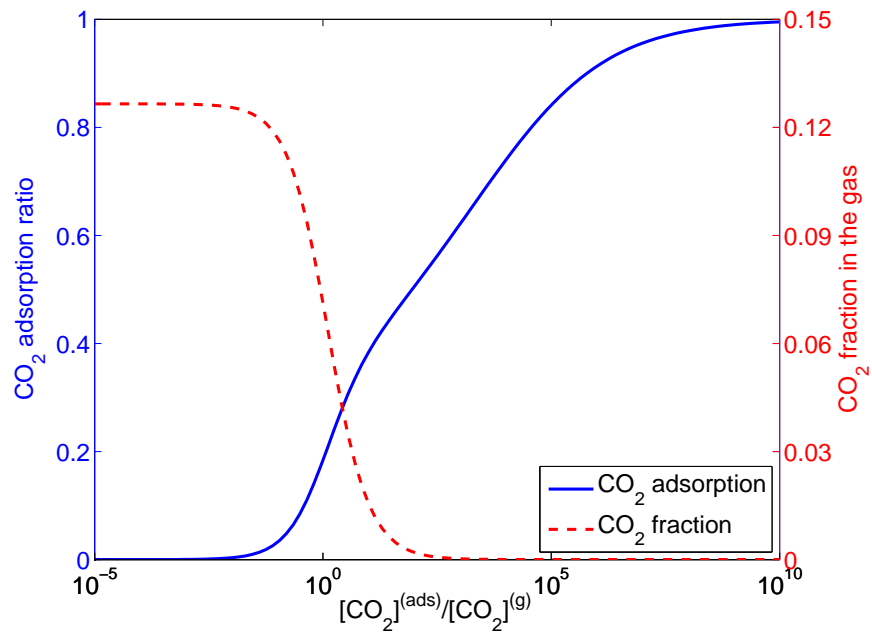


Figure 3: Actual adsorption ratio of CO_2 by the adsorbent (feed mole ratio = 1/3, $P = 5$ bar and $T = 500$ °C).

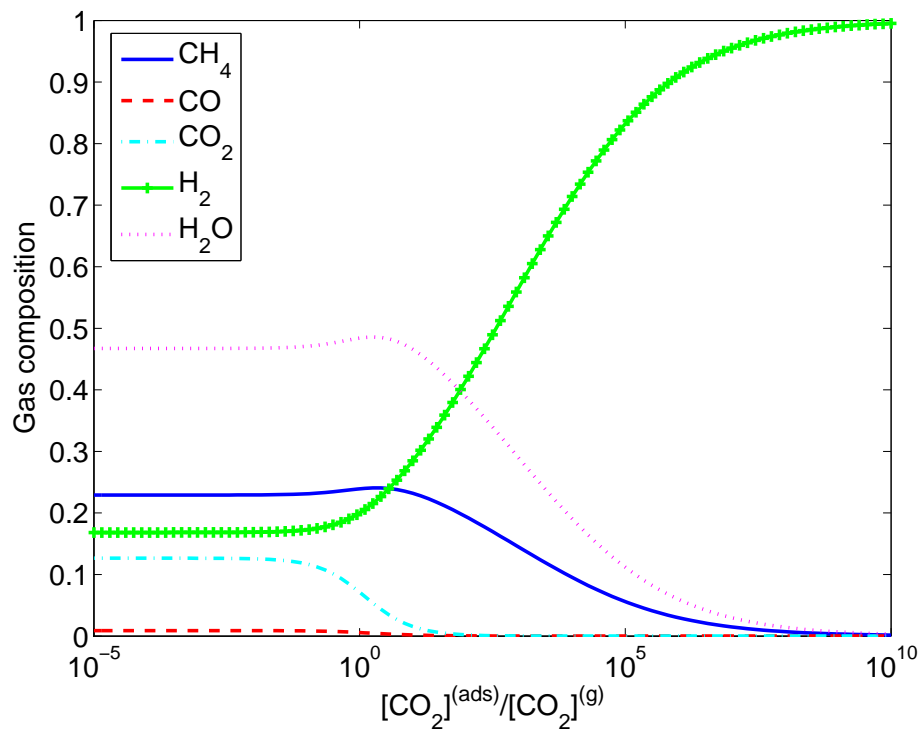


Figure 4: Composition of the gas mixture after reaction (feed mole ratio = 1/3, P = 5 bar and T = 500 °C).

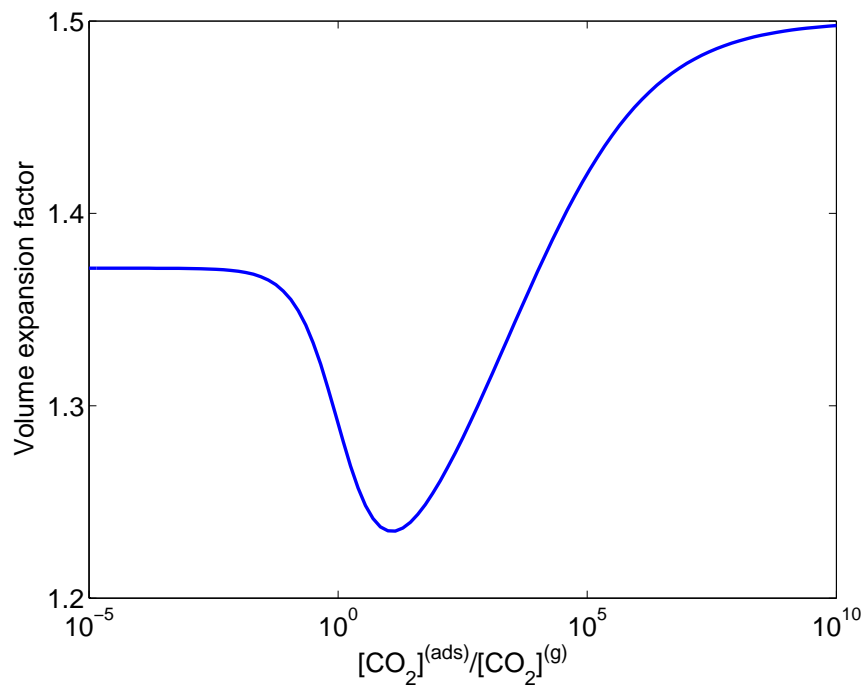


Figure 5: Volume expansion (the volume ratio of the product mixture to the reactant mixture) with respect to the reactant mixture (feed mole ratio = 1/3, $P = 5$ bar and $T = 500$ °C).

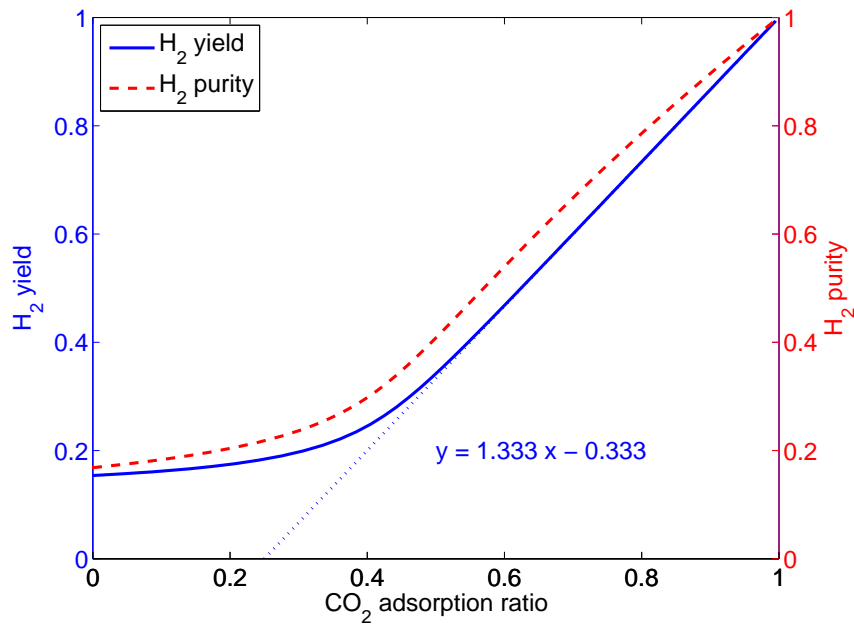


Figure 6: H₂ yield and purity as functions of the CO₂ adsorption ratio (feed mole ratio = 1/3, $P = 5$ bar and $T = 500$ °C).

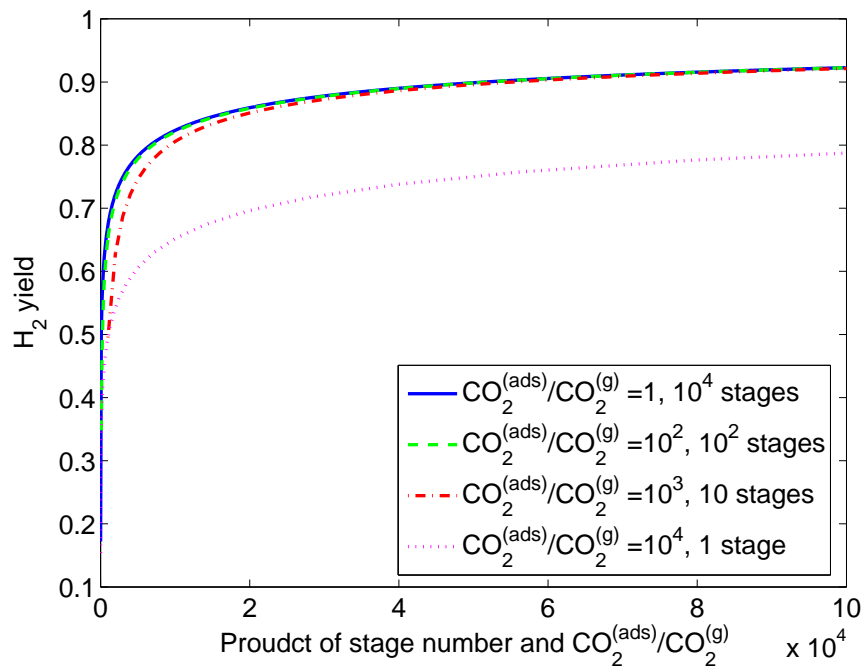


Figure 7: Conversion of $\text{C}_2\text{H}_5\text{OH}$ to H_2 (feed mole ratio = $1/3$, $P = 5$ bar and $T = 500$ °C) using different number of stages and $\text{CO}_2^{(\text{ads})}/\text{CO}_2^{(\text{g})}$ ratios.

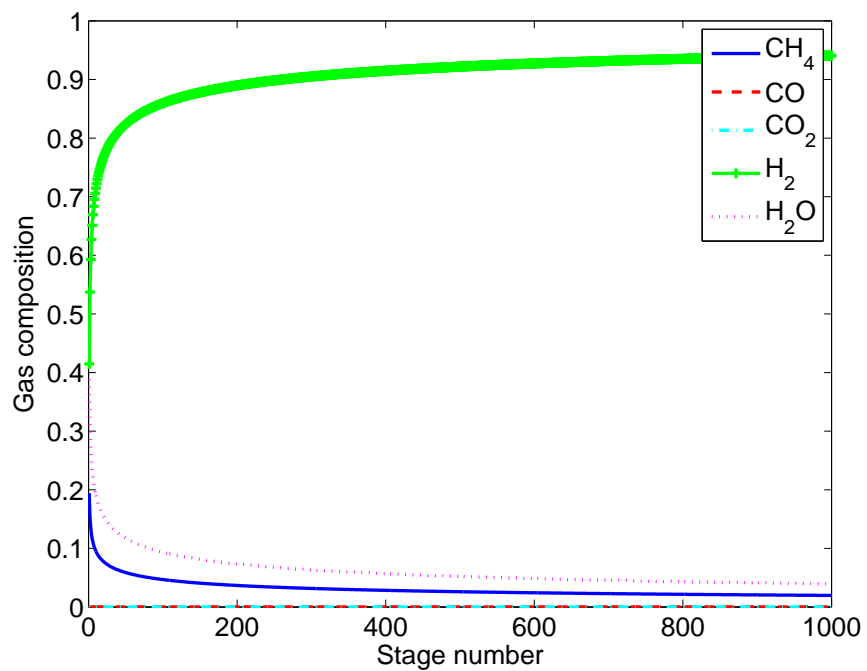


Figure 8: Composition of the gas mixture after reaction (feed mole ratio = 1/3, $P = 5$ bar and $T = 500$ °C) using multiple stages ($\text{CO}_2^{(\text{ads})}/\text{CO}_2^{(\text{g})}$ is set to be 10^2 at each stage).

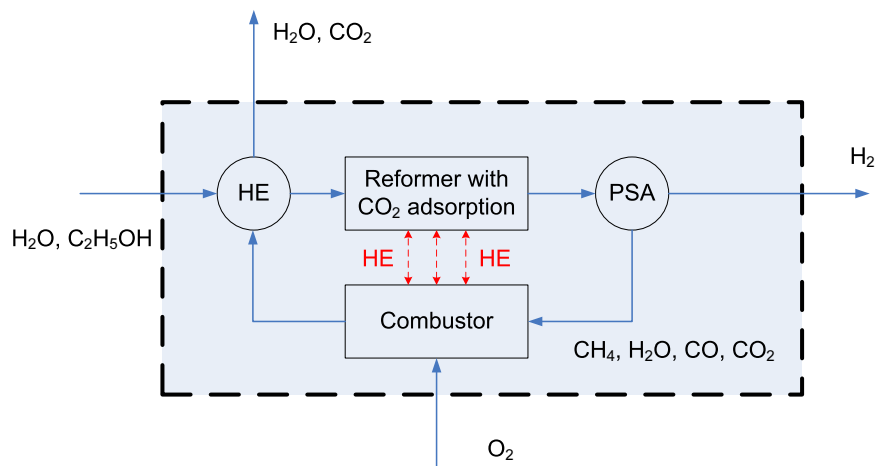


Figure 9: Integrated endothermic reforming and the exothermic combustion of unconverted CH_4 with simultaneous CO_2 in the ethanol reforming process.

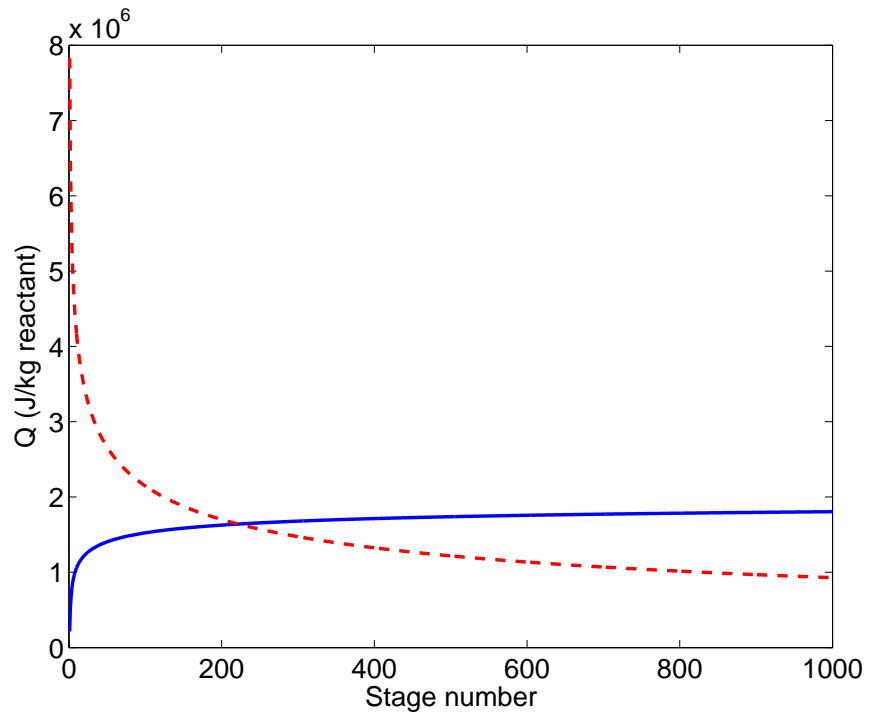


Figure 10: Heat demand by ethanol reforming v.s. heat supply through combustion of exhausting gases from the H_2 separation unit (feed mole ratio = $1/3$, $P = 5$ bar and $T = 500$ °C, $\text{CO}_2^{(\text{ads})}/\text{CO}_2^{(\text{g})} = 10^2$ at each stage).